Journal of Hydrology 590 (2020) 125449

Contents lists available at ScienceDirect

Journal of Hydrology

journal homepage: www.elsevier.com/locate/jhydrol

Research papers

Trade-off between watershed water yield and ecosystem productivity along elevation gradients on a complex terrain in southwestern China

Ning Liu[a,b,c,d], Pengsen Sun[b,*], Peter V. Caldwell[c], Richard Harper[d], Shirong Liu[b], Ge Sun[e]

[a] Department of Forest Resources, University of Minnesota, Saint Paul, MN, USA
[b] Research Institute of Forest Ecology, Environment and Protection, Chinese Academy of Forestry, Beijing, China
[c] Coweeta Hydrologic Lab, Southern Research Station, U.S. Department of Agriculture Forest Service, Otto, NC, USA
[d] College of Science, Health, Engineering and Education, Murdoch University, South Street, Murdoch, WA, Australia
[e] Eastern Forest Environmental Threat Assessment Center, Southern Research Station, U.S. Department of Agriculture Forest Service, Research Triangle Park, NC, USA

ARTICLE INFO

This manuscript was handled by Emmanouil Anagnostou, Editor-in-Chief

Keywords:
Elevation gradient
Water use efficiency
Water yield
Carbon sequestration
Trade-off

ABSTRACT

Understanding the tradeoffs between water yield and ecosystem productivity is important for developing strategies for large scale ecological restoration worldwide. This study focused on a national forest protection project in the Upper Yangtze River Basin where a logging ban was implemented in 1998. We used a hydrologic model and remote sensing data to study the interactions between water and carbon cycles along elevation gradients in the Minjiang watershed (MJ), where extensive deforestation and reforestation have occurred in the past seven decades. Average annual evapotranspiration (ET), water yield, and gross primary productivity (GPP) from 2000 to 2015 were estimated as 429 mm yr^{-1}, 555 mm yr^{-1}, and 1002 g C m^{-2} yr^{-1}, respectively. ET decreased sharply and consistently with increasing elevation, whereas GPP only decreased significantly in high elevation areas (i.e., > 3,000 m), resulting in divergent trends of water use efficiency (WUE) with elevation. Evergreen needleleaf forests (ENF) contributed 28% of water yield and 37% of GPP at the watershed scale, while grassland (GRA) also contributed 28% of water yield, but only 20% of total watershed GPP. Moreover, runoff coefficients showed strong negative correlations with GPP, suggesting a general trade-off relationship between water yield and ecosystem productivity in MJ. Our results suggest that vegetation composition and elevation played a key role in determining the relative ecological benefits for carbon and water in the study watershed with a complex terrain.

1. Introduction

There has been increasing interest in understanding interactions between water and vegetation at various scales in recent years (Jackson et al., 2005; Sun et al., 2011) under a background of dramatic global climate changes (Vasudevan et al., 2010). Carbon mitigation has been proposed to moderate climate change by increasing the capacity of carbon sinks or reducing anthropogenic carbon emissions (IPCC, 2013). Afforestation and forest restoration are two common ways to achieve carbon mitigation and reduce soil erosion. However, trade-offs between water yield and carbon sequestration have been recognized worldwide (Jackson et al., 2005; Sun et al., 2017) with implications for human water supply. For example, land cover change contributed to half of the observed change in streamflow, globally (Wei et al., 2018). Trade-offs among water, carbon, soil erosion and crop production have been documented in China for several large-scale ecological restoration projects, including the Three-North Shelterbelt Project (Deng et al., 2019) and 'Green for Grain' project (Lü et al., 2012).

Thanks to global eddy flux measurements of carbon and water, the coupling of carbon (i.e., ecosystem productivity) and water has been well established generally (Law et al., 2002; Sun et al., 2011), however few studies have examined how water yield and ecosystem productivity interact at the watershed scale in complex high elevation mountainous regions. Elevation is known to play a critical role in vegetation distribution and growth by affecting the water and solar energy supply (Liu et al., 2017; Swetnam et al., 2017; Zhou et al., 2019). For example, leaf area and total live biomass of forests vary with increasing elevation along the Qinghai-Tibet Plateau regions (Liu et al., 2017; Wang et al., 2014). These differences in vegetation and climate result in variation in watershed water balances along elevation gradients. However, patterns of water and carbon balances and the factors that determined their patterns along elevation gradients are not consistent. For example, while Hu et al. (2018) reported decreasing evapotranspiration (ET) with increasing elevation at three forested sites in Mount Gongga, Ma

* Corresponding author.
E-mail address: sunpsen@caf.ac.cn (P. Sun).

https://doi.org/10.1016/j.jhydrol.2020.125449
Received 10 April 2020; Received in revised form 16 August 2020; Accepted 20 August 2020
Available online 27 August 2020

et al. (2019) found that ET increased with increasing elevation at lower elevations and then decreased with increasing elevation at higher elevations in the northeast of the Qinghai-Tibet Plateau. Temperature changes along elevation gradients was found to be the main contributor to these variations in ET and carbon sequestration in subalpine dark coniferous forests in the southeastern Tibetan Plateau (Sun et al., 2020a, 2020b), while the dominant controls for ET switched from water to energy (shortwave radiation and air temperature) with increasing elevation in the northeastern Qinghai-Tibet Plateau (Ma et al., 2019). Clearly the patterns of water and carbon balances along elevation gradients and the factors determining their patterns for different vegetation types are complex and a comprehensive understanding of these interactions will be essential for effective environmental conservation projects.

The 24 000 km^2 Minjiang river watershed (MJ) located in the subalpine zone of the southeast edge of Qinghai-Tibet Plateau plays a strategic role in environmental protection as well as the economic and social well-being for downstream communities. The MJ experienced dramatic deforestation, with forest cover decreasing from 38.5% of the watershed in the 1950s to 23% in the 1980s (Cui et al., 2012). A series of reforestation and forest protection programs for soil conservation and water resource protection were launched in 1998, resulting in an increase in forest coverage to 34% by 2006 (Cui et al., 2012). Although forest harvesting offset the decline in annual streamflow of the Minjiang River due to climate change before 2000 (Zhang et al., 2012), streamflow has decreased significantly during the last two decades (Huang et al., 2014) due to the combined effects of climate change and forest restoration. The large scale reforestation that replaced the native fir (*Abies faxoniana*) species with spruce *(Picea asperata*) coupled with a lack of management (e.g. thinning or pruning) resulted in a two-fold increase in ET as the spruce plantations are now in their fast-growing stage (Zhang et al., 2020). Moreover, rising air temperatures have resulted in increased vegetation greening and ET (Sun et al., 2008). Understanding these changes in water and carbon balances under land use and climate change will be critical for local water resource and forest management in the MJ watershed.

The complex terrain and diverse vegetation types in MJ provide an ideal site to study the interactions between water and carbon along elevation gradients. We hypothesized that patterns of water and carbon balances and the factors that explained these patterns varied among vegetation types according to elevation gradients. Our objectives were to: (1) quantify the contribution of each vegetation type to water yield and ecosystem productivity in a watershed with complex terrain, (2) examine the sensitivity of different vegetation types to elevation with respect to their ecosystem water and carbon processes (including ET, water yield, gross primary productivity (GPP) and water use efficiency (WUE)), and (3) link vegetation composition to the relationship between water yield and carbon sequestration at the watershed scale.

2. Study area and methodology

2.1. The Minjiang watershed

The elevation of the Minjiang (MJ) watershed (30.68°N–32.83°N; 102.46°E–104.10°E) ranges from 726 m to 6118 m, with permanent snow and glaciers in the peaks of some high mountains (Fig. 1). There are two climate types in MJ, an alpine climate in high elevation catchments and a subtropical climate in low elevation catchments and downstream arid valleys. The climate of MJ was mainly affected by westerly circulation, southwest and southeast Monsoons, with a mean annual temperature of 3.5 °C (− 6.2 – 16.6 °C across the watershed) and mean annual precipitation of 990 mm yr^{-1} (750–1460 mm yr^{-1}) between 2000 and 2015. Precipitation varies spatially and temporally with sharp declines from the southwest to the northeast. The rainy season from May to October accounted for 75–90% of the total annual precipitation.

The major soil type in MJ is mountainous, brown, coniferous forest soil originating from limestone, phyllite, and basalt (Cui et al., 2012). This soil is classified as silt-loam or loam with the United States Department of Agriculture (USDA) soil texture triangle (Shirazi and Boersma, 1984), which tends to have high runoff potential (Ross et al., 2018). The soil depth ranges from 60 to 100 cm at high elevation to 160–200 cm at low elevation (Dai et al., 2013).

The main vegetation types of MJ are closed shrublands (CSH), grassland (GRA) mainly composed of alpine meadow, broadleaf and needleleaf mixed forest (MF), and evergreen needle leaf forest (ENF). Today, 40.3% of the watershed is covered by forest, mostly ENF (29.7%) and MF (6.9%). CSH and GRA account for 24.5% and 25.1% of the watershed, respectively. Ten percent of the watershed is classified as barren/built-up lands (BSV) or permanent snow/ice (SNO). Most of the vegetation in the watershed is distributed between 2500 and 4200 m elevation where water and energy availability are suitable for their growth.

2.2. Hydrologic balance modeling

ET and water yield for each vegetation type were estimated by the monthly Water Supply and Stress Index (WaSSI) hydrologic model (Sun et al., 2011). WaSSI has been broadly used across the conterminous United States for climate and water assessment (Caldwell et al., 2015; Li et al., 2020). The core of the WaSSI model is an empirical monthly ET model derived from a data set of ecosystem-level ET measurements based on eddy covariance or sapflow techniques, climate measurements, and remotely sensed leaf area index (LAI) (Sun et al., 2011) (Eq. (1)).

$$ET = 0.174 * P + 0.502 * PET + 5.31 * LAI + 0.0222 * PET * LAI \quad (1)$$

$R^2 = 0.86$, $p < 0.0001$, RMSE = 14.0 mm/month. Where PET is potential evapotranspiration calculated by Hamon's method (Hamon, 1963); LAI is mean leaf area index, and P is precipitation.

The WaSSI model compares ET demand to soil water storage using the Sacramento Soil Moisture Accounting model (SAC-SMA) (Burnash, 1995) and limits ET if soil water is insufficient to meet the demand. The basic simulation unit of the WaSSI model is a subcatchment, in which each land cover type is simulated individually. Precipitation is partitioned into effective rainfall and snow using an air temperature-based conceptual snow accumulation and melt model (McCabe and Wolock, 1999). Then effective rainfall (precipitation + snow melt) is further separated into actual ET and water yield (surface runoff and baseflow) based on the ET demand and soil water storage in the SAC-SMA model. The output of each land cover in each subcatchment is aggregated to the subcatchment and watershed scale using an area-weighted averaging scheme.

Model inputs include monthly precipitation temperature, and LAI, land cover, and soil parameters. The land cover dataset used in this study was developed using China's HJ-1A/B and Landsat dataset. The point climate data were retrieved from the Chinese Meteorological Data Sharing Service System (http://data.cma.cn/) and were interpolated to 0.01° gridded datasets by Anusplin 4.1 using the two-dimensional thin plate smoothing splines method (Hutchinson, 1998). The monthly LAI was aggregated from the Moderate Resolution Imaging Spectroradiometer (MODIS) MOD15A2H 8-day LAI product, which was reprocessed by Yuan et al. (2011).

We used methods similar to Liu et al. (2013a) to calibrate and validate the performance of the WaSSI model in the MJ watershed. Briefly, a priori soil parameters were generated from eight layer soil particle-size distribution, soil depth, and other soil property data (Dai et al., 2013) using the methods developed in Anderson et al. (2006). Streamflow measurements at the outlet of the MJ watershed at the Zipingpu gauging station (Fig. 1) were divided into a calibration period (1990–2000) and a validation period (2001–2006) to evaluate the

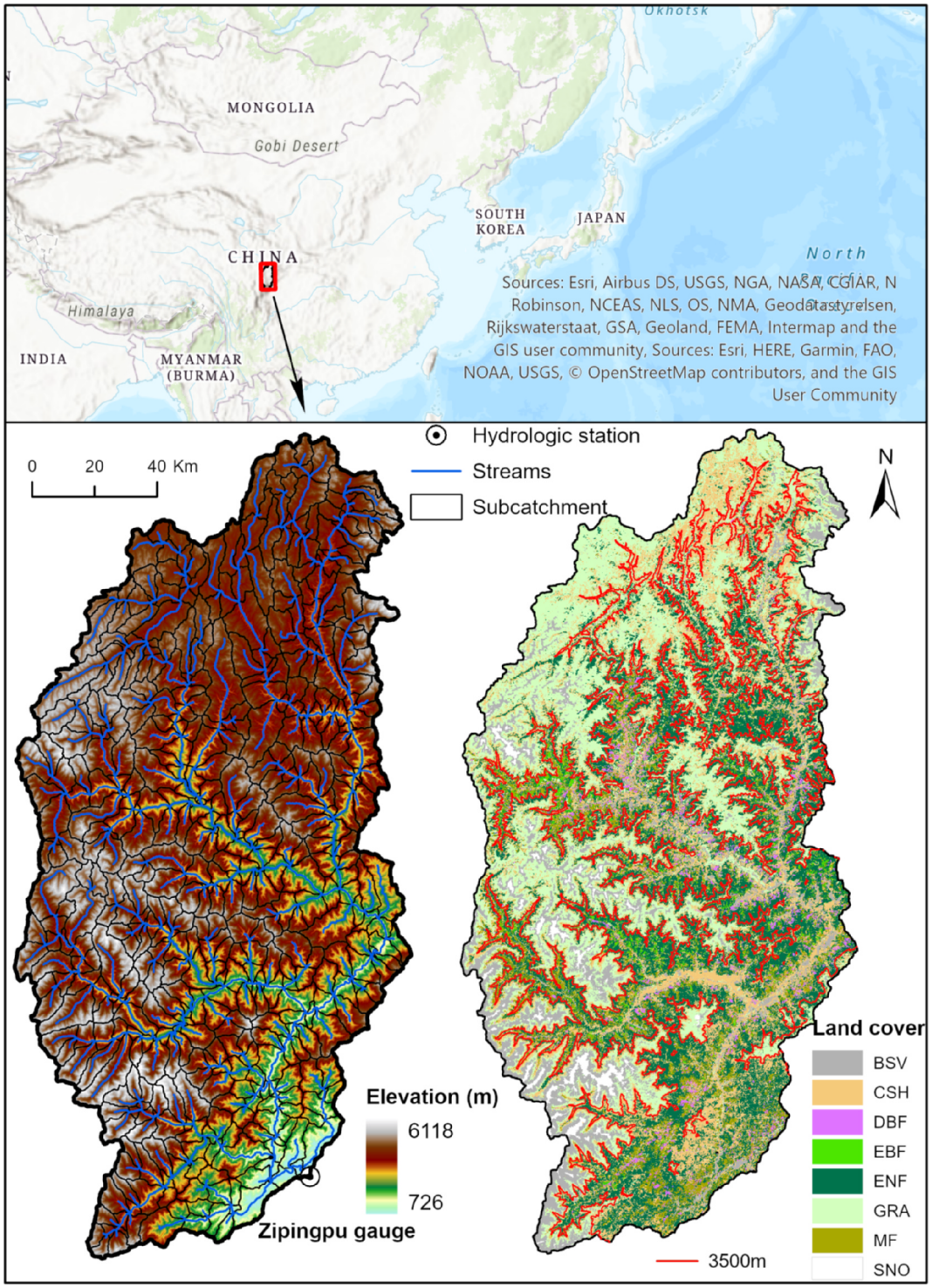

Fig. 1. The topography and spatial distribution of vegetation types of Minjiang watershed. BSV is barren or build-up area, CSH is closed shrubland, DBF is deciduous broadleaf forest, EBF is evergreen broadleaf forest, ENF is evergreen needleleaf forest, GRA is grassland (mainly is alpine meadow), MF is broadleaf and needleleaf mixed forest, and SNO is permanent snow/ice.

performance of the WaSSI model. The 11 soil parameters were adjusted to achieve the best estimate of streamflow in the calibration period, and were tested in the validation period. The watershed was divided into 537 subcatchments that were 44.7 km^2 on average based on an 85 km^2 optimal area threshold (Liu et al., 2013b) (Fig. 1). Four statistical indices, including the coefficient of determination (R^2), percent bias (%), root mean square error (RMSE, mm) and Nash–Sutcliffe model efficiency coefficient (NSE) (Nash and Sutcliffe, 1970) were calculated to assess model accuracy.

2.3. Gross primary productivity (GPP) and water use efficiency (WUE)

GPP of each vegetation type in each subcatchment was derived from the MODIS MOD17A3 annual GPP product (Zhao et al., 2005). The MOD17A3 GPP algorithm can be expressed as:

$$GPP = \varepsilon \times FPAR \times PAR \quad (2)$$

Where GPP is gross primary productivity, ε is light use efficiency, PAR is photosynthetically active radiation, and FPAR is the fraction of PAR absorbed by the vegetation canopy.

The original 500 m *500 m gridded MODIS annual GPP data was downloaded from NASA's Application for Extracting and Exploring Analysis Ready Samples (AρρEEARS) (https://lpdaacsvc.cr.usgs.gov/appeears/). The GPP of each vegetation type in each subcatchment was aggregated from the mean annual MODIS GPP from 2000 to 2015. Annual Respiration (Re) data was derived from the difference between GPP and net primary productivity (NPP), which was derived from MODIS MOD17A2 NPP data. WUE of each vegetation type in each subcatchment was defined as the ratio of gross primary productivity (GPP) to WaSSI-predicted ET.

2.4. Trade-off between water yield and GPP at the watershed scale

The relationship between runoff coefficient and GPP was used to quantify the trade-off between water yield and carbon sequestration. The ratio of water yield to precipitation (runoff coefficient) was used to quantify the water yield capacity for a subcatchment. The 537 subcatchments were divided into vegetation composition groups based on the coverage of each vegetation type to evaluate the impact of vegetation composition on water and carbon relationships. The vegetation composition group of a subcatchment was defined as the dominant vegetation type, if one existed. The dominant vegetation type in a subcatchment was assumed to be the vegetation type that comprised > 60% of the total land area. If there was no dominant vegetation type in the subcatchment, the subcatchment was assigned to the Mixed group. There were four vegetation composition groups in MJ, including CSH dominant, ENF dominant, GRA dominant, and Mixed.

3. Results

3.1. Model evaluation

The WaSSI model performed well over the calibration period (1990 to 2000) and the validation period (2001–2006) (Figs. 2 and 3). WaSSI captured the general temporal dynamics of water yield at both the monthly and annual scales, with monthly NSE of 0.78 and 0.72 for calibration and validation periods, respectively, and annual NSE of 0.73 and 0.72 for calibration and validation periods, respectively (Fig. 3). The monthly and annual simulated water yield was highly correlated to the observed water yield, with R^2 of 0.79 and 0.78, and RMSE of 15.57 mm and 35.33 mm at the monthly and annual scale during the calibration period, respectively. Similarly, R^2 was 0.75 and 0.72, and RMSE was 15.48 mm and 32.72 mm at the monthly and annual scale during the validation period, respectively (Fig. 3). Overall, the simulated water yield was very close to the observations, with a percent bias of 0.6%. However, the model overestimated water yield for months with very high precipitation in 1990, 1995, 2001 and 2003 (Figs. 2a and 3a), but underestimated water yield in 1992 and 1999, which could be related to melting of glacial snow and ice that changed the annual water balance (Liu et al., 2008). While the model considers seasonal snow melting processes, the permanent glacial snow and ice melting was not considered. The averaged ET simulated by WaSSI for the entire MJ from 2000 to 2006 was 426 mm yr^{-1}, which was very close to the difference between annual precipitation and observed water yield (415 mm yr^{-1}). Despite the differences between simulated and observed water yield for some wet months, the WaSSI model reasonably estimated water yield for the MJ watershed (Fig. 2b).

3.2. Water and carbon for different vegetation types along elevation gradients

Forests accounted for approximately 51% of GPP (Fig. 4c) and 36% of water yield while covering 40% of the watershed (Fig. 4a and d). ENF contributed the highest percentage of total watershed carbon sequestration (37%) and water yield (28%). Although GRA accounted for 25% of the land area, this land cover type contributed 20% of the total carbon sequestration while contributing the same proportion of water yield as ENF (28%). CSH occupied 25% of the land area while contributing 23% of the water yield and 26% of the carbon sequestration. The remaining forest types (MF, DBF and EBF) contributed to watershed water supply in proportion to their land coverage fraction (Fig. 4d).

Forests generally had much higher ET than nonforest land cover types (Fig. 5a). DBF ET was slightly greater than MF and EBF ET among forest types, the average of the top three forest types was about 560 mm yr^{-1}. The average ET of ENF, CSH, and GRA was 509, 487, and 429 mm yr^{-1}, respectively (Fig. 5a). As the average annual precipitation was quite similar among vegetation types (Fig. S1), water yield among land cover types exhibited the opposite pattern as ET, with water yield greatest for GRA and lowest for DBF (Fig. 5b).

Similar to ET, forest land GPP was greater than that of nonforest lands. EBF was the highest (1428 g C m^{-2} yr^{-1}), followed by DBF and MF (~1360 g C m^{-2} yr^{-1}) (Fig. 5c). ENF had the lowest GPP (1224 g C m^{-2} yr^{-1}) among forest lands but higher than CSH (1076 g C m^{-2} yr^{-1}). GRA was the lowest among all vegetation types, with an average of 762 g C m^{-2} yr^{-1}.

The difference between water yield and carbon sequestration among vegetation types relates to differences in their water use efficiency. The WUE differed among vegetation types (Fig. 5d) within a range of 1.75–2.56 g C kg^{-1} H_2O yr^{-1}. The higher-productivity forests generally had higher WUE (~2.4–2.6 g C kg^{-1} H_2O yr^{-1}) than the lower-productivity CSH (~2.2 g C kg^{-1} H_2O yr^{-1}) and GRA (~1.7 g C kg^{-1} H_2O yr^{-1}). WUE of EBF was slightly higher than other forest types.

3.3. Variation of water and carbon along elevation gradients

Spearman rank correlation was used to examine relationships between elevation and key structural, functional, and efficiency parameters involved in the water and carbon cycles. Water yield was positively related to elevation but negatively related to temperature, aridity index (potential evapotranspiration/precipitation) and vapor pressure deficit (VPD) (Fig. 6). ET was positively related to temperature, aridity index and VPD but negatively related to elevation. GPP and Re showed strong positive correlation with LAI, but slight correlation with elevation and climate variables. WUE had a strong and consistent negative relationship with temperature and aridity index, but was only slightly related to elevation (Fig. 6). Moreover, divergent correlation along elevation gradients was found for LAI, GPP, Re and WUE (green box in Fig. 6).

Breakpoints in the relationship between environmental variables and elevation were tested using the "**segmented**" package in R 3.5 (R Development Core Team, 2018). GPP and LAI had very similar relationships with elevation; these were stable for elevations below 3300 m and decreasing significantly ($p < 0.001$) for elevations above 3300 m (Tables 1 and 2). In contrast, WUE had strong elevation-dependent relationships across all elevations, and 3500 m was the threshold where the relationships reversed from positive (below 3500 m) to negative (above 3500 m) (Tables 1 and 2).

Although the breakpoints in water and carbon parameters varied among different vegetation types, the correlations between elevation and those parameters were quite similar across vegetation types (Fig. 7 and Table 2). ET was consistently and negatively correlated with elevation in all vegetation types (Fig. 7a). GPP slightly increased with increasing elevation at low elevations for most vegetation types, but significantly decreased with increasing elevation for elevations > 3000 m (Fig. 7c). LAI of most vegetation types generally showed similar negative relationships at high elevation but positive relationships at low elevation, except in the case of DBF and EBF (Fig. S2). Across all vegetation types, the relationship between elevation and WUE varied

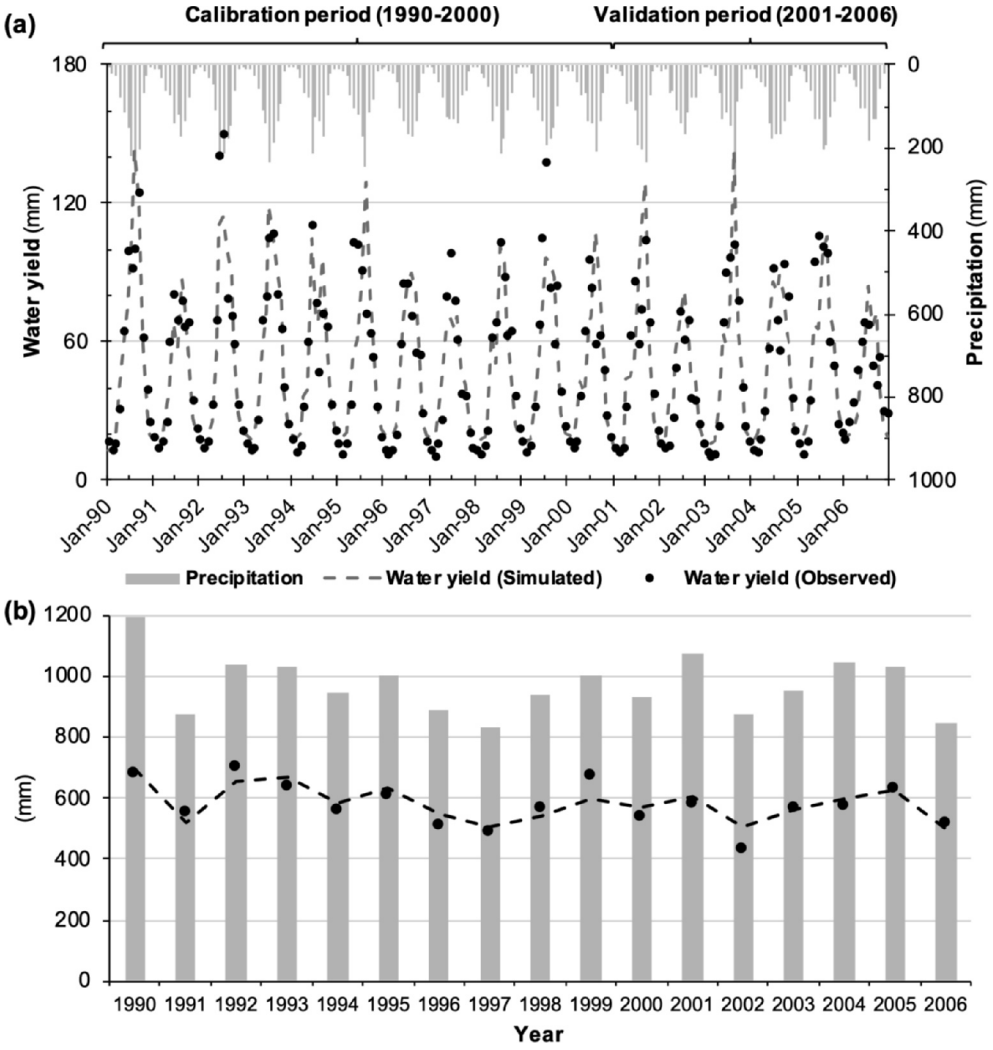

Fig. 2. Time series of monthly (a) and annual (b) simulated and observed water yield (mm) of Zipingpu hydrologic station for the calibration period (1990–2000) and the validation period (2001–2006).

according to their natural distribution pattern (Fig. 7d). For ENF, MF and CSH that were distributed across both high and low elevation areas, the increasing trend in WUE with increasing elevation began to decrease at around 3500 m (Fig. 7d, Tables 1 and 2). EBF and DBF were mostly distributed at low elevations (< 3500 m) and had a positive correlation between WUE and elevation. On the contrary, GRA was distributed mainly at high elevation (> 3000 m) and had a strong negative correlation with elevation when the elevation was higher than 3600 m.

3.4. Impact of vegetation composition on water yield and carbon sequestration at subcatchment scale

Water yield and GPP varied by dominant vegetation type and

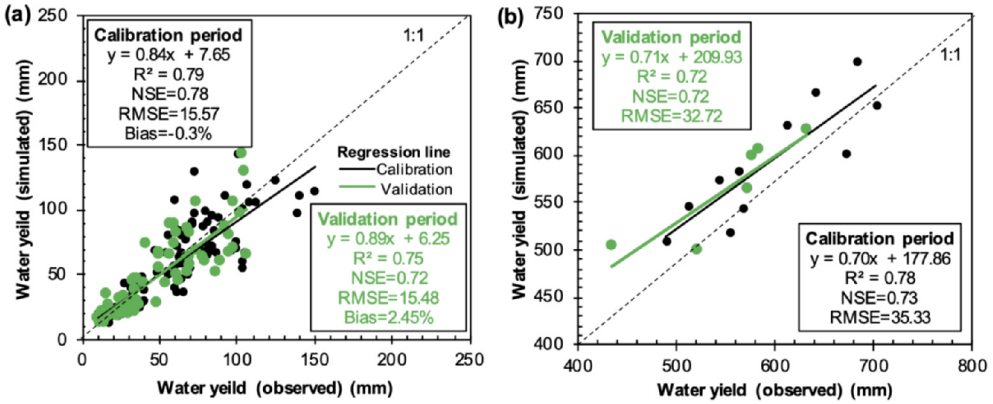

Fig. 3. Monthly (a) and annual (b) scatterplots between the simulated and observed water yield of Zipingpu hydrologic station for the calibration period (1990–2000) and the validation period (2001–2006).

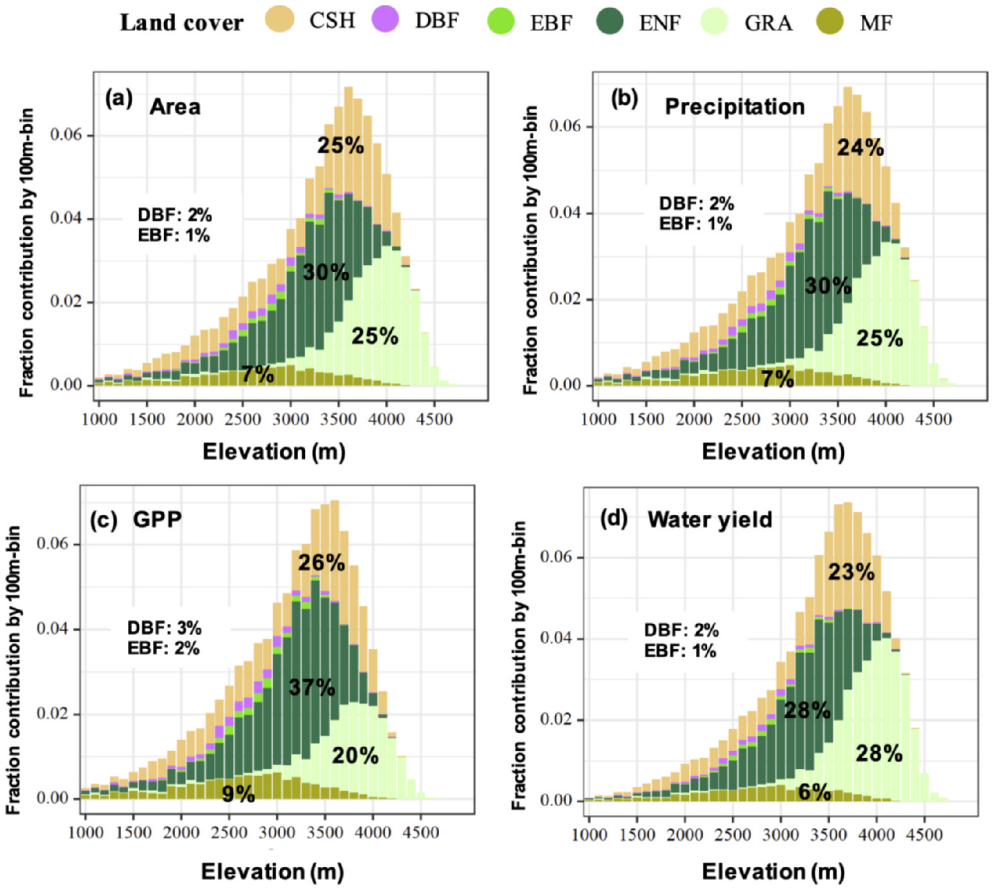

Fig. 4. Fraction of total watershed area (a), precipitation (b), gross primary productivity (c) and water yield (d) for different vegetation types in each 100-m elevation bin. Labels on the bar are the percentage of each vegetation of the total. CSH is closed shrubland, DBF is deciduous broadleaf forest, EBF is evergreen broadleaf forest, ENF is evergreen needleleaf forest, GRA is grassland, and MF is broadleaf and needleleaf mixed forest.

elevation over the 252 mixed vegetation subcatchments (Table 3). GRA dominated subcatchments in high elevation areas had the lowest carbon sequestration (GPP = 724 ± 140 g C m^{-2} yr^{-1}) and highest water yield and runoff coefficient (0.61 ± 0.07). On the contrary, ENF dominated subcatchments had the highest carbon sequestration (GPP = 1238 ± 100 g C m^{-2} yr^{-1}) but lowest runoff coefficient (0.49 ± 0.05).

Standardized (Z-score) long term average runoff coefficient and GPP exhibited a strong negative relationship when all subcatchments were pooled (Fig. 8). Moreover, negative relationships were also seen in the four vegetation composition groups independently, despite their differences in either slopes or Z-score tendencies. Opposite trends in runoff coefficient and GPP suggested a trade-off relationship between water yield and carbon sequestration, and Z-score tendency can be used to evaluate the relationship. Given the breakpoints of WUE for all vegetation types was 3500 m, we used this threshold to study the relationship between water and carbon in low and high elevation areas. There was no significant difference in Z-score tendencies among vegetation composition groups in the low elevation areas (elevation < 3500 m) (Fig. 9a). However, in high elevation areas (elevation > 3500 m), most ENF dominant subcatchments had relatively high carbon sequestration and low runoff coefficient, while most GRA dominant subcatchments showed contrasting low carbon sequestration and high runoff coefficient (Fig. 9b). Mixed and CSH dominant subcatchments generally had either relatively high runoff coefficient or carbon sequestration. Above 3500 m, ENF dominant subcatchments shift rightward and downward (Fig. 9b), while no trends were detected in CSH dominant and Mixed groups.

4. Discussion

The relationships between water and carbon, at either vegetation type or subcatchment scale, were significantly affected by elevation. As we hypothesized, we found different breakpoints for different vegetation types along elevation gradients. However, similar water and carbon relations to elevation were observed among vegetation types. Water yield showed a strong positive correlation with elevation, while GPP was divergently related to elevation between low elevation and high elevation areas.

4.1. Effects of elevation on WUE

We found that forest generally had much higher WUE than shrubland and grassland along the elevation gradients. This result is consistent with results based on ChinaFlux (Li et al., 2018; Xiao et al., 2013) and global eddy covariance measurements (Sun et al., 2011; Zhang et al., 2016). For example, the simulated WUE of GRA (1.75 ± 0.4 g C kg^{-1} H_2O yr^{-1}) in this study is similar to the observed WUE (1.72 g C kg^{-1} H_2O yr^{-1}) at the closest Haibei Alpine Tibet eddy covariance site, while the simulated WUE of DBF (2.42 ± 0.2 g C kg^{-1} H_2O yr^{-1}) in this study is close to the observed WUE (2.26 g C kg^{-1} H_2O yr^{-1}) at the nearest Hunan Yueyang eddy covariance site (Xiao et al., 2013). Similarly, the simulated WUE of ENF (2.41 ± 0.2 g C kg^{-1} H_2O yr^{-1}) is close to the range of observed WUE (2.5–3.1 g C kg^{-1} H_2O yr^{-1}) along the elevation gradient from 2800 m to 3700 m in Mountain Gongga (Sun et al., 2020a, 2020b). However, ET observed at Mount Gongga (700–780 mm yr^{-1}) (Hu et al., 2018), was higher than the simulated ET (350–750 mm yr^{-1}) in this study. This is because the mean annual precipitation in Mount Gongga is > 1600 mm yr^{-1}, which is much higher than MJ, and the observed sites are in a low elevation area (3300 m).

Vegetation composition and climate conditions along elevation gradients resulted in divergent trends in WUE between low elevation and high elevation. The breakpoint of WUE along the elevation gradient

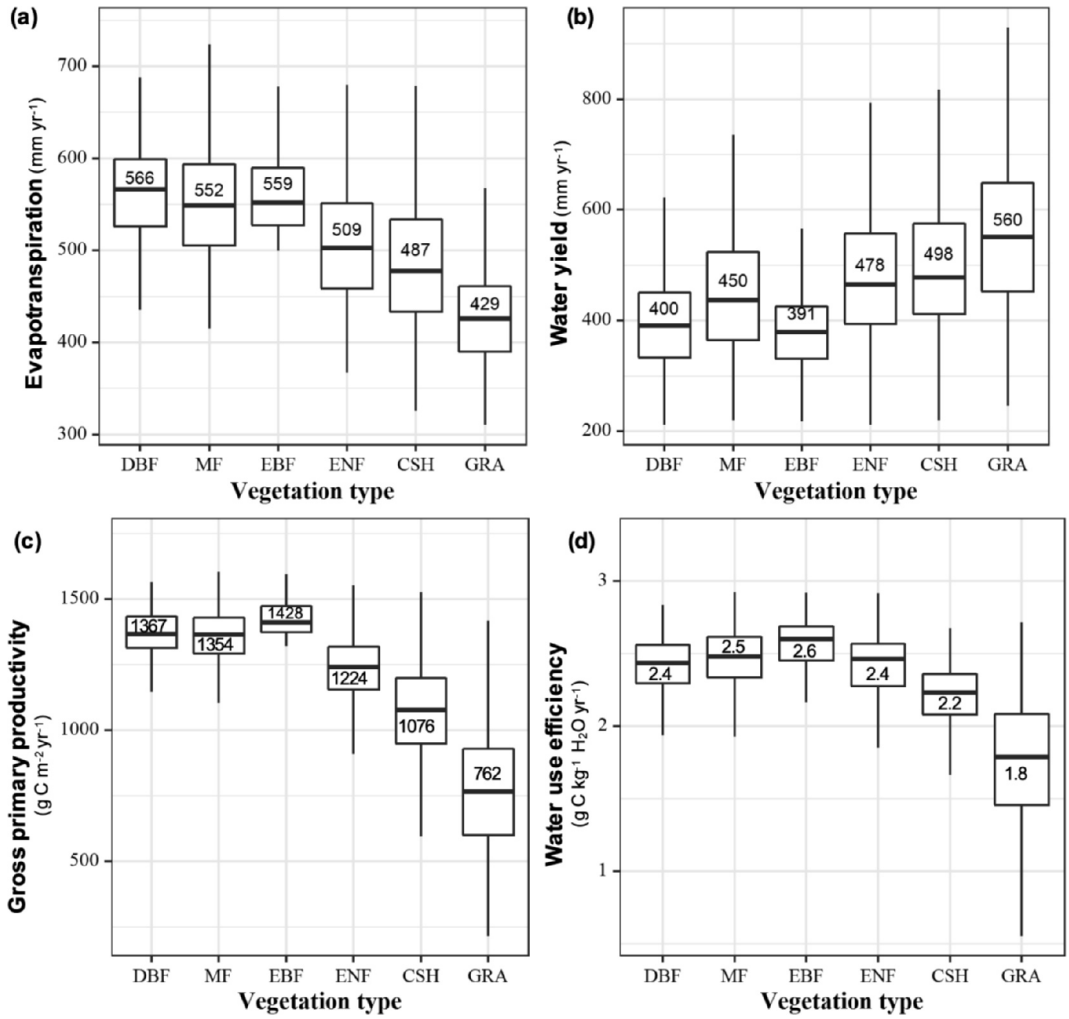

Fig. 5. Mean annual evapotranspiration (ET) (a), water yield (b), gross primary productivity (GPP) (c), and water use efficiency (WUE) (d) of each vegetation type from 2000 to 2015 in the Minjiang watershed. Labels on the boxes are the mean. CSH is closed shrubland, DBF is deciduous broadleaf forest, EBF is evergreen broadleaf forest, ENF is evergreen needleleaf forest, GRA is grassland, and MF is broadleaf and needleleaf mixed forest.

at approximately 3500 m was related to the vegetation distribution. In general, most of the forest was distributed at lower elevations, then transitioned from dark conifer forest to shrubland and grassland at around 3500 m (Cui et al., 2012; Sun et al., 2020a, 2020b). This change in vegetation composition resulted in a decrease in WUE for higher elevations. On the other hand, changes in climatic conditions with elevation resulted in a gradual change in water and carbon parameters for all vegetation types. For elevations lower than the breakpoint of WUE (3500 m), the increase in forest WUE was a result of the significant decline in ET because GPP did not change with increasing elevation (Table 2). Hu et al. (2018) reported a similar ET decline with a rate of 9.72 mm per 100 m along an elevation gradient in Mountain Gongga. In contrast to the northeast of Qinghai-Tibet where water availability limits ET in low elevation (Ma et al., 2019), we found ET was more strongly related to temperature than precipitation along elevation gradients (Fig. 6), which is similar to the result of the Zhang et al. (2020). In addition, ET for elevations between 2500 and 3500 m was not water or energy limited and thus was suitable for forest growth (Zhang et al., 2013). Therefore LAI, Re, and GPP of most of those vegetation types were not related to the elevation change in low and moderate elevation areas (Table 2 and Fig. S2). However, GPP declined along the elevation gradient in high elevation areas (> 3500 m), leading to the dramatic decrease in WUE (Table 2). Although solar radiation was higher in high elevation area than lower elevation (Fig. 6), low temperature becomes the main constraining factor for vegetation growth in high elevation areas (Xiao et al., 2013). In addition, the high precipitation at high elevation leads to lower VPD which further limits GPP (Fig. S2). Lastly, the steep slope and shallow soil associated with higher elevations also constrain the growth of vegetation (Zhang et al., 2013).

Among forest types, ENF showed the highest breakpoints along elevation (Table 1), while GRA was most sensitive to the temperature at high elevation. The negative correlation between GRA GPP with elevation ($rho = -0.84$) was much stronger than that of ENF ($rho = -0.45$). The break point of GRA GPP (~3600 m) was also higher than ENF (~3300 m). The different sensitivities and change points among vegetation types suggest potential dynamics in boundaries between vegetation types under future climate change (Gao et al., 2019) with implications for the water balance in MJ.

4.2. Trade-off between water yield and carbon sequestration

Vegetation composition determined the water use efficiency at the subcatchment scale and thus defined the relationship between water yield and carbon sequestration in MJ. The low GRA ET resulted in a high runoff coefficient but low GPP in GRA dominated subcatchments, while the high ENF ET led to the low runoff coefficient but high GPP in ENF dominated subcatchments. In general, the subcatchment benefit of water yield or carbon sequestration depends on the proportion of forest coverage, i.e. higher forest coverage leads to higher carbon

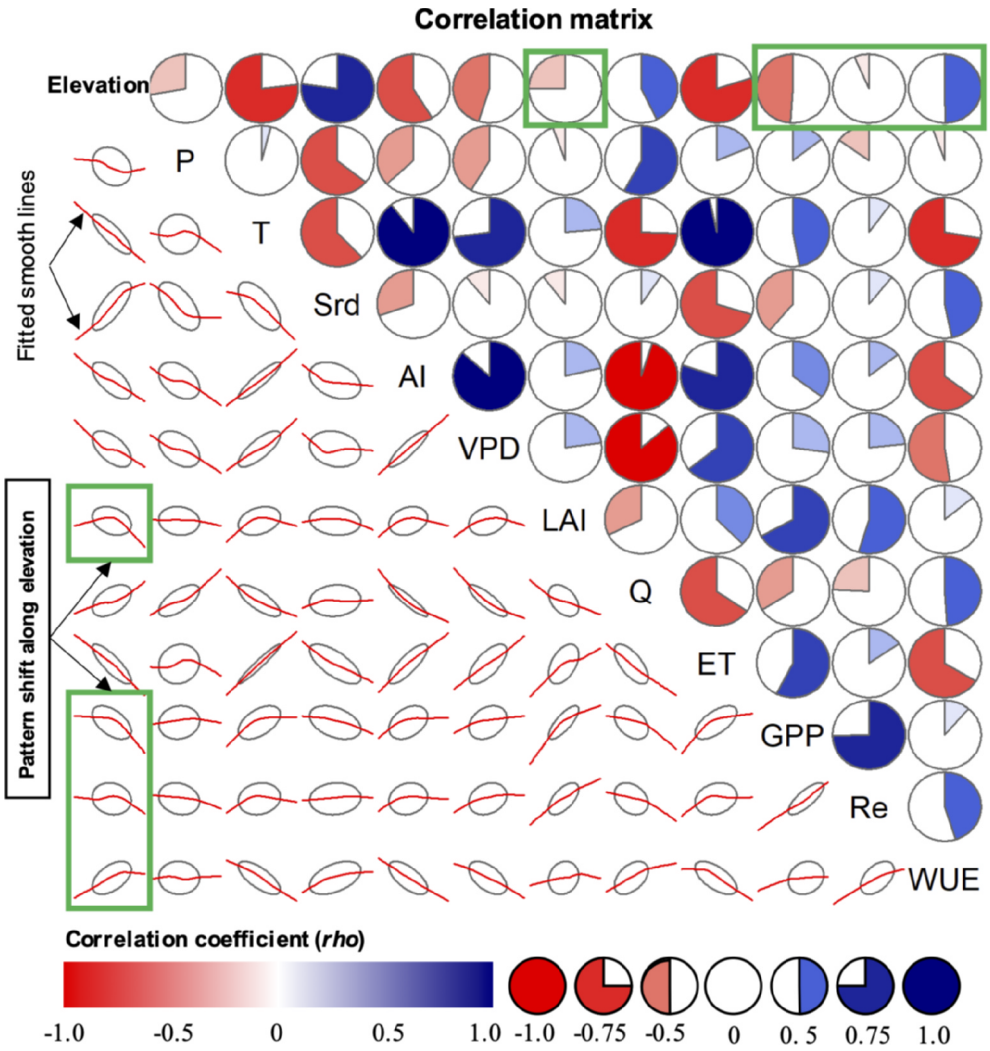

Fig. 6. Correlation matrix between elevation and climate variables (precipitation (P), temperature (T), Solar radiation (Srd), Aridity index (AI), vapor pressure deficit (VPD)), leaf area index (LAI), water yield (Q), and evapotranspiration (ET), gross primary productivity (GPP), respiration (Re) and water use efficiency (WUE) for all vegetation types. In the upper-right panel, pies reflect the Spearman's correlation coefficient (*rho*); In the lower-left panel, ellipse shows the distribution of the points with fitted smooth lines. The green box highlights some variables with two directions of the relationship of them along elevation gradients. (For interpretation of the references to colour in this figure legend, the reader is referred to the web version of this article.)

Table 1
Breakpoint of elevation for gross primary productivity (GPP), respiration (Re), water yield, and water use efficiency (WUE) across different vegetation types.

Variables	Breakpoint (m)				
	All	MF	ENF	CSH	GRA
LAI	3138	2932	3306	3312	3526
GPP	3276	2993	3317	3324	3591
Re	3406	3153	3477	3407	3519
Water yield	3617	3028	3205	3267	3300
WUE	3500	3197	3498	3372	3639

All is all vegetation types. CSH is closed shrubland, ENF is evergreen needleleaf forest, GRA is grassland, and MF is broadleaf and needleleaf mixed forest.

sequestration but lower water yield. This also can be verified by paired catchments experiments where it has been shown that deforestation leads to an increase in water yield while reforestation or plantation results in a decrease in water yield (Zhang et al., 2017). Interestingly, the diverse mixed vegetation type showed not only balanced ecological benefits for water and carbon (Fig. 8), but was also stable with respect to elevation from below 3500 m to above 3500 m (Fig. 9). This might be related to the varied water use efficiency of different vegetation types. In addition, water generally flows from low water consumption vegetation (e.g. GRA and CSH) at the ridge to high water use vegetation in the valley (forest types) (Fan et al., 2019). Therefore, managing the percentage of forest coverage and their distribution in a watershed

Table 2
The Spearman rank correlation tests of elevation against evapotranspiration (ET), gross primary productivity (GPP), respiration (Re), water yield, and water use efficiency (WUE) for different elevation ranges (All – whole range, low – lower than breakpoint, high – higher than breakpoint in Table 1).

Variables	Elevation range	No of points	*rho*				
			All	MF	ENF	CSH	GRA
ET	all	1941	−0.9	−0.85	−0.91	−0.9	−0.71
GPP	all	1941	−0.79	−0.57	−0.61	−0.67	−0.85
	lower	889	–	–	–	–	–
	higher	1052	−0.88	−0.67	−0.45	−0.69	−0.84
Re	all	1941	−0.52	−0.22	–	−0.75	0.25
	lower	1034	0.2	0.25	0.3	0.34	0.41
	higher	907	−0.79	−0.49	−0.45	−0.77	−0.28
Water yield	all	1941	0.54	0.23	0.33	0.48	0.69
	lower	1300	0.31	–	0.36	0.35	–
	higher	641	0.5	0.38	–	0.29	0.63
WUE	all	1941	−0.35	0.5	0.5	–	−0.77
	lower	1166	0.47	0.58	0.74	0.61	0.39
	higher	775	−0.84	−0.43	−0.45	−0.5	−0.8

Note: *rho* is Spearman's correlation coefficient and only showed variables with the significance *(p)* of the Spearman test is < 0.05. All is all vegetation types. CSH is closed shrubland, ENF is evergreen needleleaf forest, GRA is grassland, and MF is Broadleaf and needleleaf mixed forest.

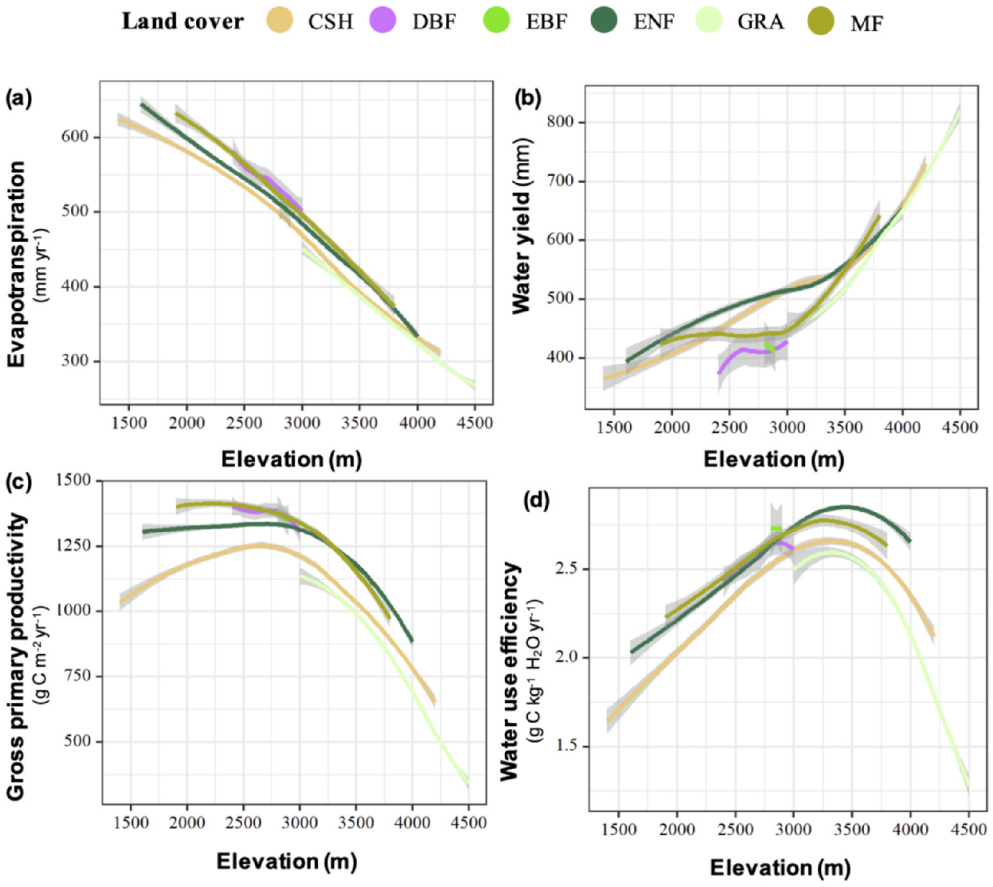

Fig. 7. Relationships between elevation and evapotranspiration (a), water yield (b), gross primary productivity (c), and water use efficiency (d) for different vegetation types. Those smooth lines for each vegetation type are plotted using "loess" method in R 3.5, with confidence interval as the shade. CSH is closed shrubland, DBF is deciduous broadleaf forest, EBF is evergreen broadleaf forest, ENF is evergreen needleleaf forest, GRA is grassland, and MF is broadleaf and needleleaf mixed forest.

Table 3
Distribution of elevation, precipitation (P), temperature (T), leaf area index (LAI), water yield (Q), gross primary productivity (GPP), and runoff coefficient (RC) for different vegetation dominant subcatchments.

Vegetation Composition group	Number of subcatchments	Elevation	P	T	LAI	Q	RC	GPP
		(m)	(mm yr^{-1})	(°C)	m^2/m^2	(mm yr^{-1})		(g C m^{-2} yr^{-1})
CSH dominant	40	2743 ± 1100	922 ± 103	6.6 ± 3.6	1.2 ± 0.2	454 ± 83	0.49 ± 0.06	1089 ± 173
ENF dominant	151	3104 ± 404	1007 ± 99	5 ± 2.2	1.5 ± 0.2	501 ± 93	0.49 ± 0.05	1238 ± 100
GRA dominant	71	3952 ± 286	942 ± 93	0.8 ± 1.6	0.8 ± 0.2	582 ± 117	0.61 ± 0.07	724 ± 140
Mixed	252	3207 ± 723	979 ± 116	4.5 ± 3.6	1.2 ± 0.3	531 ± 149	0.54 ± 0.10	1039 ± 231

CSH is closed shrubland, ENF is evergreen needleleaf forest, GRA is grassland, and Mixed is no dominant vegetation type.

could be considered in future forest management planning to maximize both water yield and carbon sequestration.

In addition to vegetation composition, ecosystem services are also affected by local climate conditions. Some subcatchments had the same trends between runoff coefficient and GPP (Fig. 8). We found that higher temperature and lower precipitation led to both low water yield and carbon sequestration of some subcatchments dominated by mixed minor vegetation types or shrublands in the valley of MJ known as the "Dry valley" (Pang et al., 2008). The low precipitation directly reduced the runoff coefficients, and high temperature increased ET which further decreased the runoff coefficient. Moreover, this increase in ET did not increase GPP because of the high aridity index in this valley area (elevation < 2000 m) (Fig. S2c). On the contrary, some ENF dominated subcatchments had both high water yield and carbon sequestration due to relatively high precipitation (Fig. 9a and Fig. S2a). However, warming could increase ET of ENF at high elevation, and this might decrease water yield in the future (Goulden and Bales, 2014).

5. Conclusions

In this study, the WaSSI model and MODIS products were used to examine the relationship between elevation and key structural, functional, and efficiency parameters associated with water and carbon cycles in MJ. A significant trade-off relationship between water yield and GPP was detected along elevation gradients in MJ, and vegetation composition appeared to play a key role in determining the relative ecological benefits for carbon and water. Along the elevation gradients, ET was significantly related to elevation change, whereas there was a divergent response in GPP between low elevation and high elevation. Apart from vegetation distribution, climate variables, especially temperature, significantly affected water yield and carbon sequestration and their interaction along elevation gradients. Managing the percentage of forest coverage and their distribution in a watershed could be considered in future forest management planning to maximize both water yield and carbon sequestration. The Qinghai-Tibet Plateau has been experiencing considerable warming, therefore future research could further investigate the sensitivity of different vegetation types to climate change and how vegetation change affects the water balance

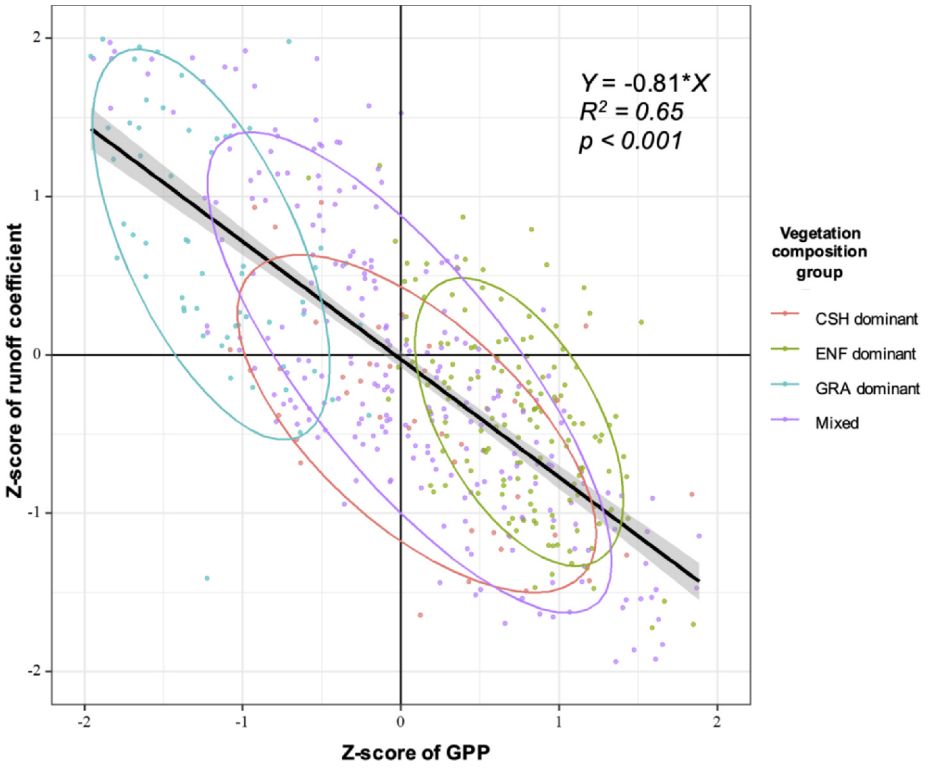

Fig. 8. The correlation between standardized (Z-score) runoff coefficient and gross primary productivity (GPP) in the Minjiang watershed. Each point represents a subcatchment. CSH is closed shrubland, ENF is evergreen needleleaf forest, GRA is grassland, and Mixed is no dominant vegetation type. The ellipse was drawn by "*stat_ellipse*" in "**ggplot**" package using R 3.5.

especially in high elevation areas.

CRediT authorship contribution statement

Ning Liu: Software, Investigation, Writing - original draft. **Pengsen Sun:** Conceptualization, Formal analysis, Writing - review & editing. **Peter V. Caldwell:** Visualization. **Richard Harper:** Validation. **Shirong Liu:** Supervision. **Ge Sun:** Methodology.

Declaration of Competing Interest

The authors declare that they have no known competing financial interests or personal relationships that could have influenced the work reported in this paper.

Acknowledgement

This study was funded jointly by the science foundation of Chinese Academy of Forestry (CAFYBB2017MA009) and the National Key R&D Program of China (2017YFC0505006) and supported by the Key Laboratory of Forest Ecology and Environment of the National Forestry and Grassland Administration, China.

Appendix A. Supplementary data

Supplementary data to this article can be found online at https://doi.org/10.1016/j.jhydrol.2020.125449.

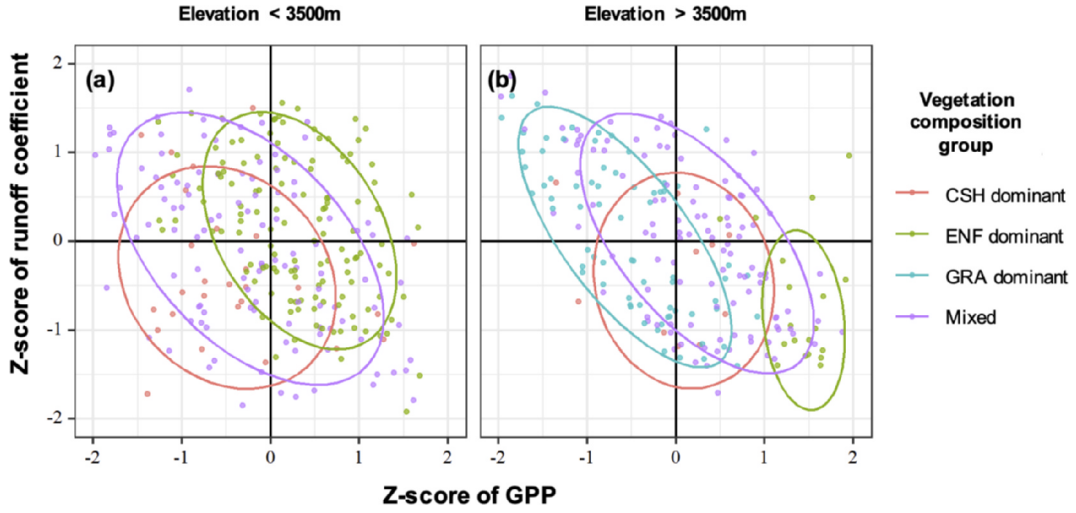

Fig. 9. The correlation between standardized (Z-score) runoff coefficient and gross primary productivity (GPP) in different elevation ranges in the Minjiang watershed. Each point represents a subcatchment. CSH is closed shrubland, ENF is evergreen needleleaf forest, GRA is grassland, and Mixed is no dominant vegetation type. The ellipse was drawn by the "*stat_ellipse*" function in "**ggplot**" package using R 3.5.

References

Anderson, R.M., Koren, V.I., Reed, S.M., 2006. Using SSURGO data to improve Sacramento Model a priori parameter estimates. J. Hydrol. 320, 103–116. https://doi.org/10.1016/j.jhydrol.2005.07.020.

Burnash, R.J.C., 1995. The NWS river forecast system. Comput. Model. Watershed Hydrol. 311–366, 311–366.

Caldwell, P.V., Kennen, J.G., Sun, G., Kiang, J.E., Butcher, J.B., Eddy, M.C., Hay, L.E., Lafontaine, J.H., Hain, E.F., Nelson, S.A.C., Mcnulty, S.G., 2015. A comparison of hydrologic models for ecological flows and water availability. Ecohydrology 8, 1525–1546. https://doi.org/10.1002/eco.1602.

Cui, X., Liu, S., Wei, X., 2012. Impacts of forest changes on hydrology: A case study of large watersheds in the upper reaches of Minjiang River watershed in China. Hydrol. Earth Syst. Sci. 16, 4279–4290. https://doi.org/10.5194/hess-16-4279-2012.

Dai, Y., Shangguan, W., Duan, Q., Liu, B., Fu, S., Niu, G., 2013. Development of a china dataset of soil hydraulic parameters using pedotransfer functions for land surface modeling. J. Hydrometeorol. 14, 869–887. https://doi.org/10.1175/JHM-D-12-0149.1.

Deng, C., Zhang, B., Cheng, L., Hu, L., Chen, F., 2019. Vegetation dynamics and their effects on surface water-energy balance over the Three-North Region of China. Agric. For. Meteorol. 275, 79–90. https://doi.org/10.1016/j.agrformet.2019.05.012.

Fan, Y., Clark, M., Lawrence, D.M., Swenson, S., Band, L.E., Brantley, S.L., Brooks, P.D., Dietrich, W.E., Flores, A., Grant, G., Kirchner, J.W., Mackay, D.S., McDonnell, J.J., Milly, P.C.D., Sullivan, P.L., Tague, C., Ajami, H., Chaney, N., Hartmann, A., Hazenberg, P., McNamara, J., Pelletier, J., Perket, J., Rouholahnejad-Freund, E., Wagener, T., Zeng, X., Beighley, E., Buzan, J., Huang, M., Livneh, B., Mohanty, B.P., Nijssen, B., Safeeq, M., Shen, C., van Verseveld, W., Volk, J., Yamazaki, D., 2019. Hillslope hydrology in global change research and earth system modeling. Water Resour. Res. 1737–1772. https://doi.org/10.1029/2018WR023903.

Gao, M., Piao, S., Chen, A., Yang, H., Liu, Q., Fu, Y.H., Janssens, I.A., 2019. Divergent changes in the elevational gradient of vegetation activities over the last 30 years. Nat. Commun. 10, 1–10. https://doi.org/10.1038/s41467-019-11035-w.

Goulden, M.L., Bales, R.C., 2014. Mountain runoff vulnerability to increased evapotranspiration with vegetation expansion. Proc. Natl. Acad. Sci. USA 111, 14071–14075. https://doi.org/10.1073/pnas.1319316111.

Hamon, W.R., 1963. Computation of direct runoff amounts from storm rainfall. Int. Assoc. Sci. Hydrol. Publ. 63, 52–62.

Hu, Z., Wang, G., Sun, X., Zhu, M., Song, C., Huang, K., Chen, X., 2018. Spatial-temporal patterns of evapotranspiration along an elevation gradient on Mount Gongga, Southwest China. Water Resour. Res. 54, 4180–4192. https://doi.org/10.1029/2018WR022645.

Huang, X., Zhao, J., Li, W., Jiang, H., 2014. Impact of climatic change on streamflow in the upper reaches of the Minjiang River. China. Hydrol. Sci. J. 59, 154–164. https://doi.org/10.1080/02626667.2013.853878.

Hutchinson, M.F., 1998. Interpolation of rainfall data with thin plate smoothing splines. Part I: two dimensional smoothing of data with short range correlation. J. Geogr. Inf. Decis. Anal. 2, 139–151 https://doi.org/10.1.1.13.6255.

IPCC, 2013. Climate Change 2013: The Physical Science Basis. Contribution of Working Group I to the Fifth Assessment Report of the Intergovernmental Panel on Climate Change, Cambridge University Press, Cambridge, United Kingdom and New York, NY, USA. https://doi.org/10.1017/CBO9781107415324.

Jackson, R.B., Jobbágy, E.G., Avissar, R., Roy, S.B., Barrett, D.J., Cook, C.W., Farley, K.A., Le Maitre, D.C., McCarl, B.A., Murray, B.C., 2005. Atmospheric science: trading water for carbon with biological carbon sequestration. Science (80-.) 310, 1944–1947. https://doi.org/10.1126/science.1119282.

Law, B.E., Falge, E., Gu, L., Baldocchi, D.D., Bakwin, P., Berbigier, P., Davis, K., Dolman, A.J., Falk, M., Fuentes, J.D., Goldstein, A., Granier, A., Grelle, A., Hollinger, D., Janssens, I.A., Jarvis, P., Jensen, N.O., Katul, G., Mahli, Y., Matteucci, G., Meyers, T., Monson, R., Munger, W., Oechel, W., Olson, R., Pilegaard, K., Paw, U.K.T., Thorgeirsson, H., Valentini, R., Verma, S., Vesala, T., Wilson, K., Wofsy, S., 2002. Environmental controls over carbon dioxide and water vapor exchange of terrestrial vegetation. Agric. For. Meteorol. 113, 97–120. https://doi.org/10.1016/S0168-1923(02)00104-1.

Li, C., Sun, G., Caldwell, P.V., Cohen, E., Fang, Y., Zhang, Y., Oudin, L., Sanchez, G.M., Meentemeyer, R.K., 2020. Impacts of urbanization on watershed water balances across the conterminous United States. Water Resour. Res. 56. https://doi.org/10.1029/2019WR026574.

Li, Y., Shi, H., Zhou, L., Eamus, D., Huete, A., Li, L., Cleverly, J., Hu, Z., Harahap, M., Yu, Q., He, L., Wang, S., 2018. Disentangling climate and LAI effects on seasonal variability in water use efficiency across terrestrial ecosystems in China. J. Geophys. Res. Biogeosci. https://doi.org/10.1029/2018JG004482.

Liu, N., Sun, P., Liu, S., Sun, G., 2013a. Coupling simulation of water-carbon processes for catchment-calibration and validation of the WaSSI-C model. Chin. J. Plant Ecol. 37, 492–502. https://doi.org/10.3724/sp.j.1258.2013.00051.

Liu, N., Sun, P., Liu, S., Sun, G., 2013b. Determination of spatial scale of response unit for WaSSI-C eco–hydrological model—a case study on the upper Zagunao River watershed of China. J. Plant Ecol. 37 (2), 132–141. https://doi.org/10.3724/sp.j.1258.2013.00014.

Liu, P., Hao, L., Pan, C., Zhou, D., Liu, Y., Sun, G., 2017. Combined effects of climate and land management on watershed vegetation dynamics in an arid environment. Sci. Total Environ. 589, 73–88. https://doi.org/10.1016/j.scitotenv.2017.02.210.

Liu, Y., Fan, N., An, S., Bai, X., Liu, F., Xu, Z., Wang, Z., Liu, S., 2008. Characteristics of water isotopes and hydrograph separation during the wet season in the Heishui River, China. J. Hydrol. 353, 314–321. https://doi.org/10.1016/j.jhydrol.2008.02.017.

Lü, Y., Fu, B., Feng, X., Zeng, Y., Liu, Y., Chang, R., Sun, G., Wu, B., 2012. A policy-driven large scale ecological restoration: quantifying ecosystem services changes in the loess plateau of China. PLoS One. https://doi.org/10.1371/journal.pone.0031782.

Ma, Y.J., Li, X.Y., Liu, L., Yang, X.F., Wu, X.C., Wang, P., Lin, H., Zhang, G.H., Miao, C.Y., 2019. Evapotranspiration and its dominant controls along an elevation gradient in the Qinghai Lake watershed, northeast Qinghai-Tibet Plateau. J. Hydrol. https://doi.org/10.1016/j.jhydrol.2019.05.019.

McCabe, G.J., Wolock, D.M., 1999. General-circulation-model simulations of future snowpack in the Western United States. J. Am. Water Resour. Assoc. 35, 12. https://doi.org/10.1111/j.1752-1688.1999.tb04231.x.

Nash, J.E., Sutcliffe, J.V., 1970. River flow forecasting through conceptual models part I - a discussion of principles. J. Hydrol. 10, 282–290. https://doi.org/10.1016/0022-1694(70)90255-6.

Pang, X., Bao, W., Wu, J., 2008. Reasons of dry valley climate characteristic and its formation reason in upstream of Minjiang River. Resour. Environ. Yangtze Basin 17, 46–53.

R Development Core Team, 2018. A Language and Environment for Statistical Computing. R Found. Stat Comput.

Ross, C.W., Prihodko, L., Anchang, J., Kumar, S., Ji, W., Hanan, N.P., 2018. HYSOGs250m, global gridded hydrologic soil groups for curve-number-based runoff modeling. Sci. Data. https://doi.org/10.1038/sdata.2018.91.

Shirazi, M.A., Boersma, L., 1984. A unifying quantitative analysis of soil texture. Soil Sci. Soc. Am. J. https://doi.org/10.2136/sssaj1984.03615995004800010026x.

Sun, G., Caldwell, P., Noormets, A., McNulty, S.G., Cohen, E., Moore Myers, J., Domec, J.-C., Treasure, E., Mu, Q., Xiao, J., John, R., Chen, J., 2011. Upscaling key ecosystem functions across the conterminous United States by a water-centric ecosystem model. J. Geophys. Res. 116, 1–16. https://doi.org/10.1029/2010jg001573.

Sun, G., Hallema, D., Asbjornsen, H., 2017. Ecohydrological processes and ecosystem services in the Anthropocene: a review. Ecol. Process. https://doi.org/10.1186/s13717-017-0104-6.

Sun, J., Sun, X., Hu, Z., Wang, G., 2020a. Exploring the influence of environmental factors in partitioning evapotranspiration along an elevation gradient on Mount Gongga, eastern edge of the Qinghai-Tibet Platea, China. J. Mt. Sci. 17, 384–396. https://doi.org/10.1007/s11629-019-5687-1.

Sun, P., Liu, S., Jiang, H., Lü, Y., Liu, J., Lin, Y., Liu, X., 2008. Hydrologic effects of NDVI time series in a context of climatic variability in an Upstream Catchment of the Minjiang River. J. Am. Water Resour. Assoc. 44, 1132–1143. https://doi.org/10.1111/j.1752-1688.2008.00256.x.

Sun, X., Wang, G., Huang, M., Chang, R., Hu, Z., Song, C., Sun, J., 2020b. The asynchronous response of carbon gain and water loss generate spatio-temporal pattern of WUE along elevation gradient in southwest China. J. Hydrol. 581. https://doi.org/10.1016/j.jhydrol.2019.124389.

Swetnam, T.L., Brooks, P.D., Barnard, H.R., Harpold, A.A., Gallo, E.L., 2017. Topographically driven differences in energy and water constrain climatic control on forest carbon sequestration. Ecosphere. https://doi.org/10.1002/ecs2.1797.

Vasudevan, D., Chua, E.Y.D., Davey, C.A., 2010. Crystal structures of nucleosome core particles containing the “601” strong positioning sequence. J. Mol. Biol. 403, 1–10. https://doi.org/10.1016/j.jmb.2010.08.039.

Wang, G., Ran, F., Chang, R., Yang, Y., Luo, J., Jianrong, F., 2014. Variations in the live biomass and carbon pools of Abies georgei along an elevation gradient on the Tibetan Plateau, China. For. Ecol. Manage. https://doi.org/10.1016/j.foreco.2014.06.023.

Wei, X., Li, Q., Zhang, M., Giles-Hansen, K., Liu, W., Fan, H., Wang, Y., Zhou, G., Piao, S., Liu, S., 2018. Vegetation cover—another dominant factor in determining global water resources in forested regions. Glob. Chang. Biol. 24, 786–795. https://doi.org/10.1111/gcb.13983.

Xiao, J., Sun, G., Chen, J., Chen, H., Chen, S., Dong, G., Gao, S., Guo, H., Guo, J., Han, S., Kato, T., Li, Y., Lin, G., Lu, W., Ma, M., McNulty, S., Shao, C., Wang, X., Xie, X., Zhang, X., Zhang, Z., Zhao, B., Zhou, G., Zhou, J., 2013. Carbon fluxes, evapotranspiration, and water use efficiency of terrestrial ecosystems in China. Agric. For. Meteorol. 182–183, 76–90. https://doi.org/10.1016/j.agrformet.2013.08.007.

Yuan, H., Dai, Y., Xiao, Z., Ji, D., Shangguan, W., 2011. Reprocessing the MODIS Leaf Area Index products for land surface and climate modelling. Rem. Sens. Environ. 115, 1171–1187. https://doi.org/10.1016/j.rse.2011.01.001.

Zhang, L., Sun, P., Liu, S., 2020. Growing-season transpiration of typical forests in different succession stages in subalpine region of Western Sichuan, China. Linye Kexue/Scientia Silvae Sin. 56, 1–9. https://doi.org/10.11707/j.1001-7488.20200101.

Zhang, M., Liu, N., Harper, R., Li, Q., Liu, K., Wei, X., Ning, D., Hou, Y., Liu, S., 2017. A global review on hydrological responses to forest change across multiple spatial scales: importance of scale, climate, forest type and hydrological regime. J. Hydrol. https://doi.org/10.1016/j.jhydrol.2016.12.040.

Zhang, M., Wei, X., Sun, P., Liu, S., 2012. The effect of forest harvesting and climatic variability on runoff in a large watershed: the case study in the Upper Minjiang River of Yangtze River basin. J. Hydrol. 464–465, 1–11. https://doi.org/10.1016/j.jhydrol.2012.05.050.

Zhang, W., Ning, J., Song, K., Li, X., Wang, Y., 2013. The response of vegetation cover to the variation of heat and water conditions in Upper Minjiang Watershed, China. J. Mt. Sci. 31, 280–286.

Zhang, Y., Song, C., Sun, G., Band, L.E., McNulty, S., Noormets, A., Zhang, Q., Zhang, Z., 2016. Development of a coupled carbon and water model for estimating global gross primary productivity and evapotranspiration based on eddy flux and remote sensing data. Agric. For. Meteorol. 223, 116–131. https://doi.org/10.1016/j.agrformet.2016.04.003.

Zhao, M.S., Heinsch, F.A., Nemani, R.R., Running, S.W., 2005. Improvements of the MODIS terrestrial gross and net primary production global data set. Rem. Sens. Environ. 95, 164–176. https://doi.org/10.1016/j.rse.2004.12.011.

Zhou, D., Hao, L., Kim, J.B., Liu, P., Pan, C., Liu, Y., Sun, G., 2019. Potential impacts of climate change on vegetation dynamics and ecosystem function in a mountain watershed on the Qinghai-Tibet Plateau. Clim. Change. https://doi.org/10.1007/s10584-019-02524-4.